Journal of Hydrosciences and Environment
ISSN: 2345-5608

Modeling dam break on an erodible bed by the moving particle semi-implicit method with exponential Herschel-Bulkley rheology

E. Jafari Nodoushan[1, *], M. Tajnesaie [2]

*1, *. Assistant Professor, Department of Civil Engineering, Bijar Branch, Islamic Azad University, Bijar, Iran (Corresponding author).*
2, Assistant Professor, Department of Civil Engineering, Bijar Branch, Islamic Azad University, Bijar, Iran.

ARTICLEINFO

Article history:

Received: 11 Aug 2020
Accepted: 06 Nov 2020

Keywords:
Moving particle semi-implicit method
Multiphase model
Exponential Herschel-Bulkley model
Erodible-bed dam break

ABSTRACT

The flow caused by a dam break usually develops towards the river or the plain flood. The downstream of the dam is usually a natural river where the bed is mobile and significant amounts of bed sediments are transferred downstream due to the non-continuous flow caused by the flood. Accurate prediction of complexities, involved in such a multiphase water-sediment system is still an important challenge for conventional mesh-based numerical models. Numerical methods, based on mesh-free Lagrangian approaches including Smoothed Particle Hydrodynamic (SPH) and Moving Particle Semi-implicit method (MPS), have provided a unique opportunity to deal with the deformation and fragmentation in these complex multiphase systems. This study develops and evaluates a mesh-free Lagrangian model based on a weakly-compressible MPS formulation for the simulation of two-phase rapid sediment transport. To model non-cohesive sediments, the sediment material is considered a non-Newtonian visco-plastic fluid, and an exponentially-regularized Herschel-Bulkley (H-B) rheological model in combination with Mohr-Coulomb yield criteria is employed. The capability of the developed numerical method is evaluated for two-phase sediment transport in a dam break on an erodible bed. Dam break flow over an erodible sediment bed for two geometrical setups (with dry and wet downstream) is considered. The comparison of the results with the available experimental measurements showed the capabilities of the proposed model in the accurate prediction of sediment and water profiles for this sample problem.

1. Introduction

Rapid sediment transport is part of many studies because it is used in many geophysical and engineering problems. The erodible-bed dam break, scouring, and sedimentation in dam reservoirs, as well as landslides under the sea, are common examples of rapid sediment transport characterized by a rapid flow of dense granular materials. Rapid flow could be initiated by an erosive flood flow (e.g., in rivers and coastal areas) or under powerful outer forces (e.g., gravity in sliding). These flow systems are characterized by high interfacial deformations and fragmentations and complex rheological behavior.

Traditionally, numerical modeling of sediment transport has been based on empirical or semi-empirical relationships (e.g. Meyer-Peter and Müller, 1948; Van Rijn, 1984). Two-phase models, in which the sediment phase acts as a separate phase, have proven to be useful for many sediment transport simulations. These methods are based either on continuum-based mesh-based Eulerian (e.g., FEM or FVM) (McTigue, 1981; Hsu et al., 2003) or on discrete Lagrangian (such as discrete element method, DEM) (Calantoni et al., 2004). The first class, though being successful in some cases, has problems in dealing with flows with large interfacial deformations (Shakibaeinia and Jin, 2011). The methods of the second class are computationally expensive for large-scale problems as they deal with the individual sediment grains. The mesh-free particle (Lagrangian) methods developed for continuum mechanics such as Smoothed Particle Hydrodynamics (SPH) by Gingold and Monaghan (1977) and Moving Particle Semi-implicit (MPS) method by Koshizuka and Oka (1996) provide an opportunity for dealing with the complexities involved in rapid sediment transport problems. Due to their mesh-free Lagrangian nature, these methods can handle large interfacial deformations. Furthermore, they do not have the scalability issue of discrete-based models as they model continuum.

The MPS method is a fully Lagrangian model originally developed for fluid mechanic problems. Gotoh and Sakai (2006) developed a multiphase MPS model for the simulation of problems with liquid-gas or liquid-solid

* Corresponding author's email: eh.jafari@iau.ac.ir

DOR: 20.1001.1.23455608.2020.4.8.5.6

phases, sediment transport, and buoyant particles. Ataei-Ashtiani and Farhadi (2006) compared different kernel functions and proposed a relationship to increase the stability of the MPS model. Khayyer and Gotoh (2009, 2010) worked on the improvement of unphysical pressure fluctuations associated with the MPS method. Shakibaeinia and Jin (2010) developed a weakly compressible MPS (MPS-WC) method for the simulation of 2D open-boundary free-surface flows. They showed that this method not only depresses unphysical fluctuations of the MPS method but also increases the efficiency and accuracy of the model in comparison with the original MPS method. Shakibaeinia and Jin (2012a) proposed a multiphase MPS method for multi-density multi-viscosity systems. By combining their multiphase MPS model with various rheological relations, they extended the application of their model to solid-liquid multiphase flows (Shakibaeinia and Jin, 2011, 2012b). Jafari-Nodoushan et al. (2016) developed a meshless Lagrangian (particle) method based on the weakly compressible MPS formulation and analyzed it for the simulation of flow over spillways. Also, Jafari-Nodoushan et al. (2018) and Tajnesaie et al. (2018) developed and characterized a multiphase WC-MPS model for gravity-driven sediment flows. Jafari et al. (2019) developed and evaluated a multiphase mesh-free particle model based on the weakly compressible MPS formulation for the simulation of sediment scouring. Recently, Jandaghian et al. (2021) developed a generalized rheology model for viscous and inertial regimes of the granular flows.

The present research aimed to develop a mesh-free model based on multiphase MPS-WC for the simulation of two-phase rapid sediment transport. A regularized visco-plastic rheological model is applied to predict the non-Newtonian behavior of the sediment phase, and the Mohr-Coulomb yield criteria with a dynamic effective pressure are used to compute the yield stress above which sediment materials start to move. The model is validated for an erodible-bed dam break test. The available experimental data are used to validate the simulated results.

2. Materials and Methods

2.1. Flow Equations

The governing equations for a weakly-compressible flow system, including mass and momentum conservation and motion in Lagrangian coordinates, are as follows:

$$\begin{cases} \dfrac{\mathrm{D}\rho}{\mathrm{D}t} + \rho\nabla\cdot\mathbf{u} = 0 & \textit{Mass conservation} \\ \rho\dfrac{\mathrm{D}\mathbf{u}}{\mathrm{D}t} = -\nabla p + \nabla\cdot\boldsymbol{\tau} + \rho\mathbf{g} & \textit{Momentum conservation} \\ p = f(\rho) & \textit{Equation of state} \\ \dfrac{\mathrm{D}\mathbf{r}}{\mathrm{D}t} = \mathbf{u} & \textit{Lagrangian Motion} \end{cases} \quad (1)$$

where $\mathbf{u}$ is the velocity vector, t is the time, ρ is the density, p is the pressure, $\mathbf{g}$ is the gravity acceleration, $\mathbf{r}$ is the position vector, and $\boldsymbol{\tau}$ is the shear stress tensor. An equation of state is used to calculate pressure using a density field. Considering the multiphase system of water and sediments as a multi-density multi-viscosity system, the governing equations are valid for both phases without applying extra forces (Shakibaeinia and Jin, 2012a).

2.2. Rheology of sediment

The system of fluid and sediments is a multiphase of solids and liquid where both phases are treated as a continuum. To calculate the viscous term in the momentum equation, the dynamic viscosity of each particle (solid or liquid phase) is required. The liquid phase (i.e., water) has a known and constant viscosity (independent of time and stress). However, the determination of solid-phase viscosity is not simple. A simple method for the caculation of solid-phase viscosity is to assume the sediment-phase behavior as a Newtonian fluid. This assumption cannot simulate the behavior of sediment flow accurately (Shakibaeinia and Jin, 2011). Therefore, the non-Newtonian behavior of the sediment phase must be considered in which the sediment behaves as a solid for stresses less than the yield stress and as a viscous fluid for stresses exceeding the yield stress (Mitsoulis, 2007). Bingham plastic, as well as Herschel–Bulkley generalized visco-plastic models for more complex cases, are extensively used to describe the behavior of sediment flow. In Herschel–Bulkley model, the shear stress tensor is calculated using a stress-dependent effective viscosity given by Papanastasiou (1987):

$$\boldsymbol{\tau} = 2\mu_{eff}E \rightarrow \mu_{eff} = \begin{cases} \dfrac{\tau_y}{2\|\mathbf{E}\|} + \mu_0\left(\|\mathbf{E}\|\right)^{N-1} & \|\tau\| > \tau_y \\ \infty & \|\tau\| < \tau_y \end{cases} \quad (2)$$

in which

$$\mathbf{E} = \frac{1}{2}\left(\nabla\mathbf{u} + (\nabla\mathbf{u})^T\right) \quad (3)$$

$$\|\mathbf{E}\| = \sqrt{I_E} = \sqrt{\frac{1}{2}\mathbf{E}:\mathbf{E}}$$

$$\|\boldsymbol{\tau}\| = \sqrt{I_\tau} = \sqrt{\frac{1}{2}\boldsymbol{\tau}:\boldsymbol{\tau}}$$

$$\tau_y = p_{mech}\sin\phi$$

where $\boldsymbol{\tau}$ and $\mathbf{E}$ are shear stress and rate of deformation tensors (with magnitudes of $\|E\|$ and $\|\tau\|$), respectively, μ_0 and N are flow consistency and behavior indices (function of grain shape and size) determined experimentally, I is the second constant of the tensor, τ_y is the yield stress determined using Mohr-Coulomb criterion for non-cohesive sediments, p_{mech} is the mechanical pressure (normal stress between the sediment grains), and N=1 shows linear behavior (Bingham plastic model).

The original form of the Herschel–Bulkley model (Eq. 2) is discontinuous when the shear rate approaches zero ($\|\mathrm{E}\| \rightarrow 0$). To avoid this and also to avoid the determination of yield regions ($\|\tau\| > \tau_y$) and non-yield

regions ($\|\tau\| \le \tau_y$), a continuous regularized form of the equation proposed by Papanastasiou (1987) is used as:

$$\mu_{eff} = \frac{\tau_y(1-\exp(-m\|\mathbf{E}\|)}{2\|\mathbf{E}\|} + \mu_0(\|\mathbf{E}\|)^{N-1} \quad (4)$$

where the parameter m controls the exponential growth of the stress. This equation is valid for both yield and non-yield regions. For stresses less than the yield stress, in which $\|\mathbf{E}\|$ approaches zero, regular effective viscosity B-P (N=1) reaches a maximum value of $\mu_{max} = \mu_0 + m\tau_y$. A schematic comparison of ideal and regularized shear stress/effective viscosity (for different values of m) is shown in Figure 1.

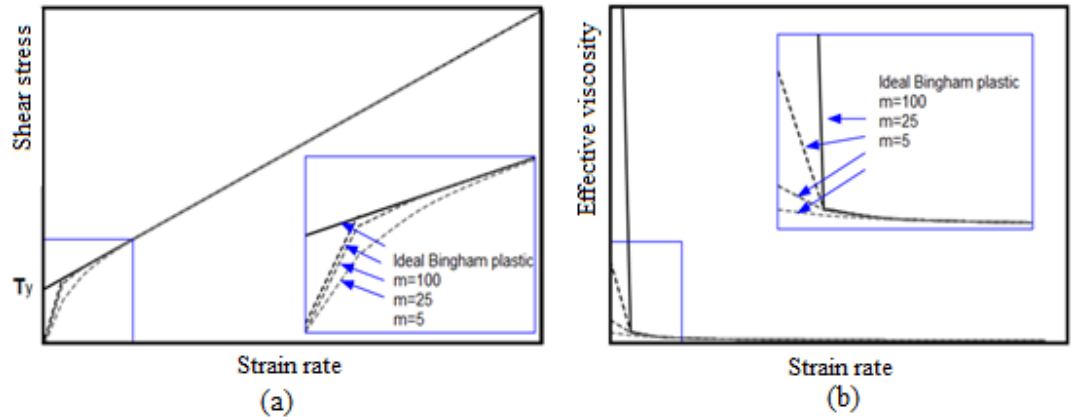


Fig. 1. A schematic comparison of (a) regular shear stress and (b) effective viscosity (for different values of m)

2.3. MPS method

In MPS, as a Lagrangian method, the solution field is divided into a set of free-to-move particles. Each particle possesses a set of field variables, and the governing equations are discretized and solved over these particles (Figure 2). Interpolation discretization of spatial derivatives is based on weight averaging (particle smoothing) between a particle of interest and its neighboring particles, located within a radius of influence, r_e. Using this weight-averaging process, the spatial derivatives are transformed to equations of particle interactions. The effect of a neighboring particle j (with Poisson vector $\mathbf{r}_j$) on the particle of interest i (with position vector $\mathbf{r}_i$) is determined using the weight (smoothing) function $W(r_{ij},r_e)$ where $r_{ij}=|\mathbf{r}_j - \mathbf{r}_i|$ is te distance between particles i and j.

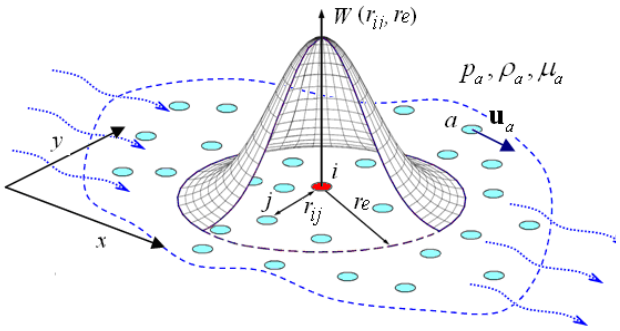


Fig. 2. A schematic of the MPS discretization method (Shakibaeinia and Jin, 2011)

A dimensionless parameter n (namely, particle number density) is used to show the density of particles around a specified particle (Shakibaeinia and Jin, 2010).

$$\langle n \rangle_i = \sum_{j \ne i} W(r_{ij}, r_e) \quad (5)$$

Assuming that all particles have equal mass (M), the smoothed value of fluid density for particle i is given by:

$$\langle \rho \rangle_i = \frac{\sum_{i \ne j} M_i W(r_{ij}, r_e)}{\int_v W(r, r_e)dv} = \frac{M}{\int_v W(r, r_e)dv}\langle n \rangle_i = \frac{\rho \langle n \rangle_i}{n_0} \quad (6)$$

where n_0 is the average initial particle number density and $\langle - \rangle$ is the weight-averaging (particle smoothing) operator. The kernel function used in this study is a third-order polynomial function defined by Shakibaeinia and Jin (2010) as follows:

$$W(r_{ij}, r_e) = \begin{cases} (1 - r_{ij}/r_e)^3 & 0 \le (r_{ij}/r_e) < 1 \\ 0 & (r_{ij}/r_e) \ge 1 \end{cases} \quad (7)$$

Note that the third-order polynomial kernel function was first proposed by Shakibaeinia and Jin (2010) to avoid inaccuracy of the second-order bell-shaped polynomial function and singularity of the rational function (two conventional MPS kernel functions).

2.3.1. MPS discretization

The gradient, divergence, and Laplacian terms in the flow governing equations need to be discretized over the particle domain. The MPS gradient of an arbitrary quantity ϕ is achieved by weighted averaging of gradient vectors between the particle of interest *i* and each of its neighboring particles as:

$$\left\langle \nabla \phi \right\rangle_i = \frac{d}{n_0} \sum_{i \neq j} \left[\frac{\phi_i - \phi_j}{r_{ij}} \frac{\mathbf{r}_j - \mathbf{r}_i}{r_{ij}} W(r_{ij}, r_e) \right] \quad (8)$$

Similarly, the divergence of the arbitrary vector **u** is given by:

$$\left\langle \nabla \cdot \mathbf{u} \right\rangle_i = \frac{d}{n_0} \sum_{i \neq j} \left[\frac{\mathbf{u}_i - \mathbf{u}_j}{r_{ij}} \cdot \frac{\mathbf{r}_j - \mathbf{r}_i}{r_{ij}} W(r_{ij}, r_e) \right] \quad (9)$$

where *d* is the space dimension. Laplacian (and vector Laplacian) is calculated by weighted averaging of diffusion of physical properties from particle *i* to its neighboring particles as:

$$\left\langle \nabla^2 \mathbf{u} \right\rangle_i = \frac{2d}{\lambda n_0} \sum_{i^1 j} \left[(\mathbf{u}_i - \mathbf{u}_j) W(r_{ij}, r_e) \right] \quad (10)$$

where λ is defined by:

$$\lambda = \frac{\int_v W(r, r_e) r^2 dv}{\int_v W(r, r_e) dv} \approx \frac{\sum_{j \neq i} r_{ij}^2 W(r_{ij}, r_e)}{\sum_{j^1 i} W(r_{ij}, r_e)} \approx \left\langle r_{ij}^2 \right\rangle \quad (11)$$

2.3.2. Calculation of pressure

The weakly compressible MPS (MPS-WC) method assumes the fluid to be slightly compressible and calculates the pressure of each particle using a stiff equation of state. In this study, Tait's state equation (commonly applied for high-pressure water flow) is used (Shakibaeinia and Jin, 2010):

$$p_i = \frac{\rho c_0^{\,2}}{\gamma} \left[\left(\frac{\langle \rho \rangle_i}{\rho_0} \right)^{\gamma} - 1 \right] = \frac{\rho c_0^{\,2}}{\gamma} \left[\left(\frac{\langle n \rangle_i}{n_0} \right)^{\gamma} - 1 \right] \quad (12)$$

where $\gamma = 7$, c_0 is a synthetic sound speed. Since using the actual sound speed results in very small time steps, a synthetic smaller sound speed is used. To keep the density variations of the liquid ($\rho/\rho\Delta$) to less than 1% of the reference density, the sound velocity should be more than 10 times the maximum fluid velocity ($|u|_{max}$).

2.4. Implementation of rheological model

To calculate the divergence of shear stress tensor ($\nabla.\boldsymbol{\tau}$), the effective viscosity, μ_{eff}, of each particle is needed (τ=2 μ_{eff} **E**). The effective viscosity of the solid phase (sediments) is obtained from the rheological model while a constant value is used for particles of the liquid phase (i.e. water). The effective viscosity for particle *i* is calculated as:

$$\left(\mu_{eff}\right)_i = \begin{cases} \dfrac{\left(\tau_y\right)_i \left(1 - exp(-m \left\| \mathbf{E} \right\|_i)\right)}{2 \left\| \mathbf{E} \right\|_i} + \mu_0 \left(\left\| \mathbf{E} \right\|_i \right)^{N-1} & i \in Solid\ phase \\ \mu_i & i \in Liquid\ phase \end{cases} \quad (13)$$

The MPS estimation of th strain-rate tensor is given by:

$$\mathbf{E}_i = \begin{bmatrix} \dot{\varepsilon}_{xx} & \dot{\varepsilon}_{xy} \\ \dot{\varepsilon}_{yx} & \dot{\varepsilon}_{yy} \end{bmatrix}_i = \frac{1}{n_0} \times \sum_{i \neq j} \frac{W(r_{ij}, r_e)}{r_{ij}^2} \begin{bmatrix} 2(u_j - u_i)(x_j - x_i) & (u_j - u_i)(y_j - y_i) + (v_j - v_i)(x_j - x_i) \\ (u_j - u_i)(y_j - y_i) + (v_j - v_i)(x_j - x_i) & 2(v_j - v_i)(y_j - y_i) \end{bmatrix} \quad (14)$$

To calculate critical shear stress (τ_y), the normal stress or mechanical pressure, p_{mech}, between the sediment phase grains is needed. For incompressible conditions, the normal stress between dry sediment grains is equal to the thermodynamic pressure *p* used in the momentum equation and given by the equation of state (for submerged materials, the pore pressure, p_{pore}, must be subtracted). The MPS method is, however, known to be associated with some unphysical pressure fluctuations. These fluctuations (though small) could introduce some unphysical vibrations, which affect the yield behavior of the sediment material. To avoid this problem, some of the recent studies on MPS and SPH (Shakibaeinia and Jin, 2011; Manenti et al., 2011) have used a hydrostatic pressure (for cases where vertical acceleration is small enough in the granular flow), written as:

$$\left(p_{mech}\right)_i = \rho_b g h_i - p_{pore} = \left(\rho_b - \rho_f\right) g h_i \quad (15)$$

where h_i is the vertical distance (in direction of gravity vector) of particle *i* and the particle at the solid-liquid interface. When the vertical acceleration of sediment material is not negligible, hydrostatic pressure is not applicable. Therefore, this study uses the thermodynamic pressure, calculated from the equation of state. But, to minimize the effect of unphysical pressure fluctuations, the smoothed value of pressure is used as:

$$\left(p_{mech}\right)_i = \left\langle p \right\rangle_i - p_{pore} = \sum_{i^1 j} p_j W(r_{ij}, r_e) - p_{pore} \quad (16)$$

2.5. Shear stress divergence

Shear stress tensor has been given by Eq. (3). The incompressible divergence of shear stress tensor for particle *i* is given by:

$$\left(\nabla.\boldsymbol{\tau}\right)_i = \mu_{eff}\nabla^2\mathbf{u}_i \qquad (17)$$

When two particles *i* and *j*, with different effective viscosities of μ_i and μ_j, are interacting, the interaction effective-viscosity (their friction coefficient) is a value in-between the two effective viscosities. The harmonic mean for this interaction viscosity is recommended as $\mu_{ij}=2\mu_j\mu_j/(\mu_i+\mu_j)$ (Shakibaeinia and Jin, 2011c). Substituting this interaction viscosity in the above equation, the divergence of the shear stress tensor for particle *i* is equal to:

$$\left\langle \nabla\cdot\boldsymbol{\tau}\right\rangle_i = \left\langle \mu_{ij}\nabla^2\mathbf{u}_i\right\rangle = \qquad (18)$$

$$\frac{4d}{\lambda n_0}\sum_{j\neq i}\left(\frac{\mu_i\mu_j}{\mu_i+\mu_j}\left(\mathbf{u}_j-\mathbf{u}_i\right)W\left(r_{ij},r_e\right)\right)$$

2.6. Boundary conditions

2.6.1. Free surface

In the MPS method, the value of particle number density is used to locate the free surface particles. Since there are no particles in the space above the free surface, particles' density decreases on the free surface (see Figure 3). A particle will be determined as a free-surface particle if its particle number density is less than a reference density. This limit depends on the problem at hand and may vary from 80% to 99% of the initial average particle number density as shown by Eq. (19). The particle's pressure on the free surface will be set to be free surface pressure (here zero). This paper has used a β value of 0.94 (recommended by Shakibaeinia and Jin, 2010).

$$\left\langle n\right\rangle_i \leq n^0\beta \qquad (19)$$

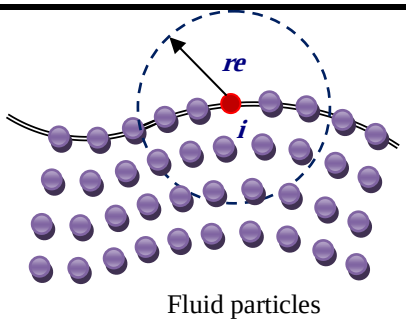


Fig. 3. Particles on the free surface

2.6.2. Solid boundary

For solid (impermeable) boundaries, such as walls or beds, this boundary condition is applied. In the neighborhood of solid boundaries, the density of particles decreases, which results in a drop in pressure and attractive force toward the solid boundary. Therefore, some fixed ghost particles are set outside the boundary to prevent this unwanted density deficiency. This method was first applied by Koshizuka et al. (1995). The solid boundaries are set as several layers of ghost particles outside of the fluid field (Figure 4). The thickness of the fictitious-particles layer depends on the radius of influence *i* (Koshizuka et al., 1996). The pressure value of these ghost particles is extrapolated from the particles located at the solid boundary (wall particles). This creates a zero pressure gradient condition at the boundary and repels particles from their solid boundaries.

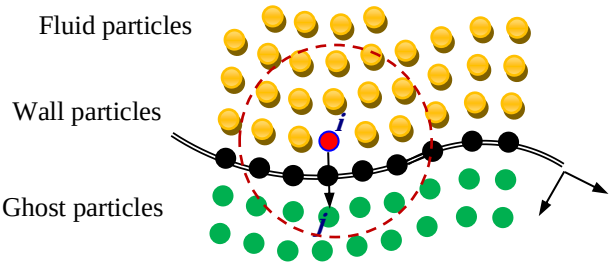


Fig4. Particles on the solid boundary and fictitious particles

2.7. Time integration and solution algorithm

To solve the governing equations, each time step is divided into two pseudo time steps of prediction and correction steps. The velocity at a new time step (*k*+1) is the sum of the predicted velocity ($\mathbf{u}^*$) and the corrected velocity ($\mathbf{u}'$):

$$\mathbf{u}_i^{k+1} = \mathbf{u}_i^* + \mathbf{u}'_i \qquad (20a)$$

where

$$\mathbf{u}_i^* = \mathbf{u}_i^k + \frac{\Delta t}{\rho_i}\left(\mathbf{g}+\mu_{ij}\nabla^2\mathbf{u}_i^k - \left(1-\alpha\right)\nabla p_i^k\right) \qquad (20b)$$

$$u' = -\frac{\alpha\,\Delta t}{\rho_i}\nabla p_i^{k+1} \qquad (20c)$$

where α is a relationship factor between 0 and 1. Particles are displaced based on the predicted velocity, and the predicted value of the particle number density n^* is

calculated. n^* is, then, used to calculate the pressure from the equation of state. The pressure gradient term is, then, recalculated and used to calculate the corrected velocity. The final solution algorithm, used for each time step, is summarized as follows:

1. Input the initial properties of the particles r_i, u_i, p_i, ρ_i, μ_i.
2. Time integration
   - Calculation of effective viscosity of each particle, μ_{eff} (for particles of solid phase, Eq. 13 is used)
   - Prediction of velocity u^* by Eq. (20b) and calculation of $\mathbf{r}^*$ and n^*
   - Calculation of pressure by Eq. (12)
   - Calculation of corrected velocity of Eq. (20c) using pressure gradient term of Eq. (8)
   - Calculation of velocity, the position of particles (moving particles with own velocity), and numerical density of particles
   - Calculation of volume fraction for concentration
   - Sending the new results ($\mathbf{r}_i^{k+1}$, $\mathbf{u}_i^{k+1}$, p_i^{k+1}, c_i^{k+1}) and preparation for the next time step.
3. Iteration for the next time step

The stability condition of Courant-Friedrichs-Lewy (CFL) should be satisfied. This condition is calculated as:

$$\Delta t \le \frac{C\Delta l}{c_0 + |U|_{\max}} \qquad (23)$$

where Δl is the distance between the particles (size of the particles) and $0 < C \le 1$ is the Courant number.

3. Results and Discussion

3.1. Dam break on an erodible bed

Dam break on an erodible bed causes the transport of sediments deposited in the reservoir to lower reaches of the river and variations in the river bed. The nature and behavior of two-phase flows (liquid-solid) are different from one-phase flows. Studying the velocity and behavior of these flows, due to the existence of suspended settable particles, is complicated. One of the most difficult problems in the simulation of two-phase flows is the great density difference between the phases. In this part of the paper, the models proposed for the simulation of the dam break on an erodible bed and the investigation of the mechanisms of morphodynamic processes are executed. For the validation purpose, the physical model of Spinewine (2005) is simulated and analyzed.

Here, the dam break flow over an erodible sediment bed for two geometrical setups (with dry and wet downstream) is considered. A prismoidal dam reservoir bounded by solid walls and a removable gate is originally full of water and sediments. The gate is removed rapidly and the wave propagates downstream. A two-dimensional schematic of the physical model, the dimensions, and the values of different rheological and numerical parameters are shown in Figure 5 and Tables 1 and 2.

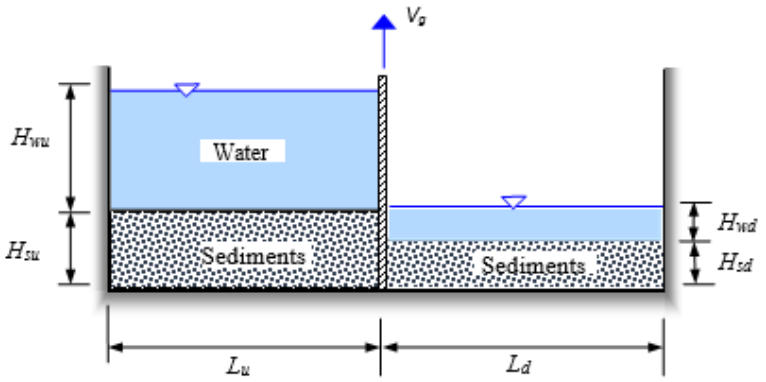


Fig. 5. A schematic design of the flow model containing sediments due to the dam break

Table 1. The geometry and dimensions of the studied physical models

Setup	Downstream length of reservoir (L_d)	Reservoir length (L_u)	Depth of downstream sediments (H_{sd})	Depth of reservoir sediments (H_{su})	Depth of downstream water (H_{wd})	Depth of water in reservoir (H_{wu})
A	3	1	0.1	0.2	0	0.25
B	3	1	0.1	0.2	0.1	0.25

Table 2. The rheological characteristics of the bed sediments

Internal friction angle of particles (°)	Bulk density (kg/m^3)	Grain density (kg/m^3)	Equivalent diameter d_{50} (m)	Sediment material
30	1892	2500	0.01	Sand

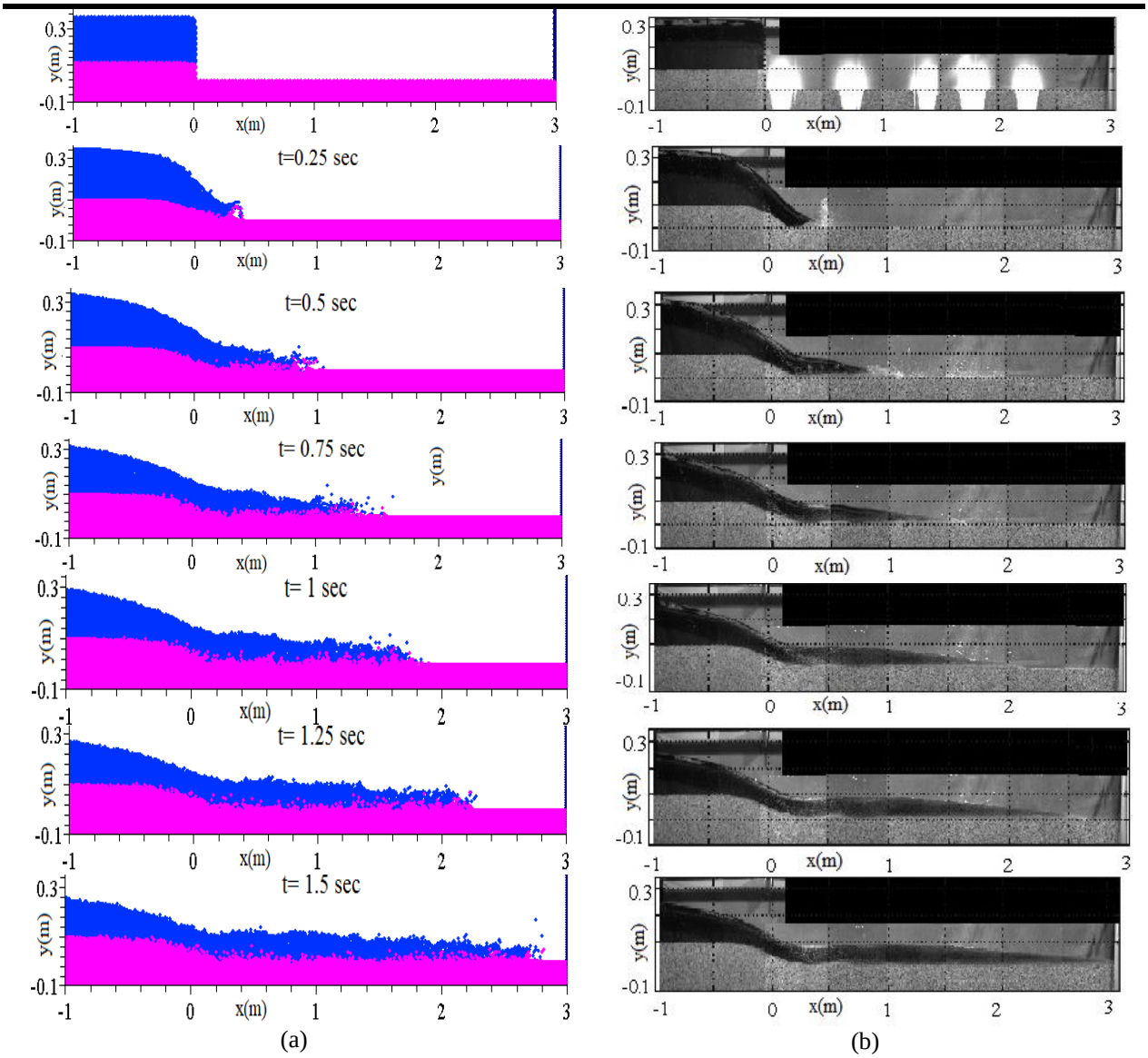


Fig. 6. (a) Numerical and (b) experimental (Spinewine, 2005) snapshots of erodible-bed dam break (setup A)

In these models, the average distance of the particles ($\Delta 1$) is taken as 0.01 m resulting in a total of 19314 particles for the dry-downstream model and 22304 particles for the wet-downstream model. The flow behavior and consistency indices, N and μ_0, are set to be 0.3 and 1, respectively (Jafari-Nodoushan et al., 2018). The simulation was performed for 1.5 seconds.

The numerical and experimental snapshots for the erodible-bed dam break (setup A) are compared in Figure 6, showing good compatibility in both free surface and sediment surface profiles. After the gate removal, a water wave forms and propagates downstream. The wave erodes the bed sediments and creates a slope near the gate location. The sediments are deposited further downstream as the wave front loses its energy.

To mitigate the possible dangers of dam breaks, it is important to calculate and predict flood wave velocity. Figure 7 shows the numerical velocity vectors. Based on the size of velocity vectors, one can distinguish three flow layers including a high-velocity water layer, a low-velocity (yielded) sediment layer (i.e. active layer), and a relatively stagnant (un-yielded) sediment layer, hidden under the active layer.

The active sediment layer is visible at earlier time steps and gradually disappears as time goes on as the result of the decrease in erosive force.

To provide a quantified comparison, the measured and simulated water/sediment profiles are plotted in Figure 8 for different times. As the figure shows, the profiles are quite compatible. The wavefront location and the erosion/ deposition pattern are very close in experimental observation and numerical results.

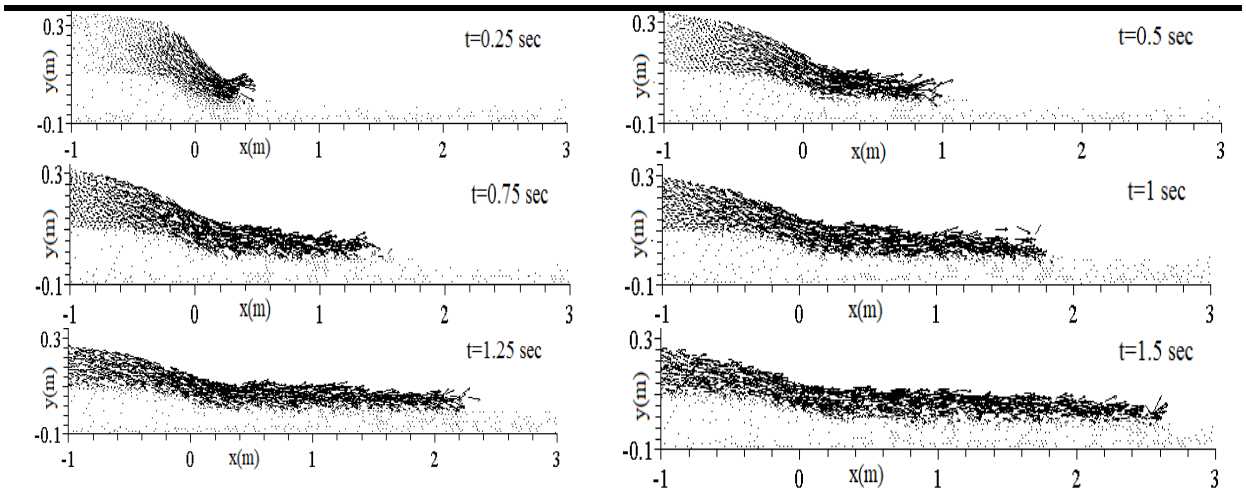


Fig. 7. The simulated velocity vectors after 0.25, 0.5, 0.75, 1, 1.25 and 1.5 seconds(Setup A)

The root mean square error (RMSE) presented in Figure 9 also shows the comparison of the water surface and sediment surface of the numerical model with the experimental model.

As can be seen in Figure 9, the scatter of the results of the present numerical method is insignificant compared to the experimental results, and its error rate averages 0.01, which indicates the accuracy of the numerical model in simulating water and sediment surface.

Figure 10 compares the numerical and experimental snapshots for erodible-bed dam breaks (setup B). Unlike setup A, in this setup, there is water downstream of the removable gate, thereby forcing the flood wave to break as it propagates downstream. The results showed that the proposed model has been able to accurately reproduce the complicated water and sediment surface profiles.

Figure 11 provides a sample snapshot of the simulated pressure, velocity magnitude/vector, and volume fraction at t=0.25 sec. The velocity and pressure have relatively smooth profiles, even near the sediment–water interface.

The maximum velocity occurred near the water wave-front, and a near-zero-velocity region can be distinguished for sediment-hidden layers. The sediment phase near the wave-front was affected by the shear stress from the water phase creating a low-velocity zone in the sediments. This zone represents the area in which the shear stress has overcome the yield stress of the sediments. In general, the results of these simulations showed the capability of the proposed model for predicting a highly erosive flow such as the erodible-bed dam break problem.

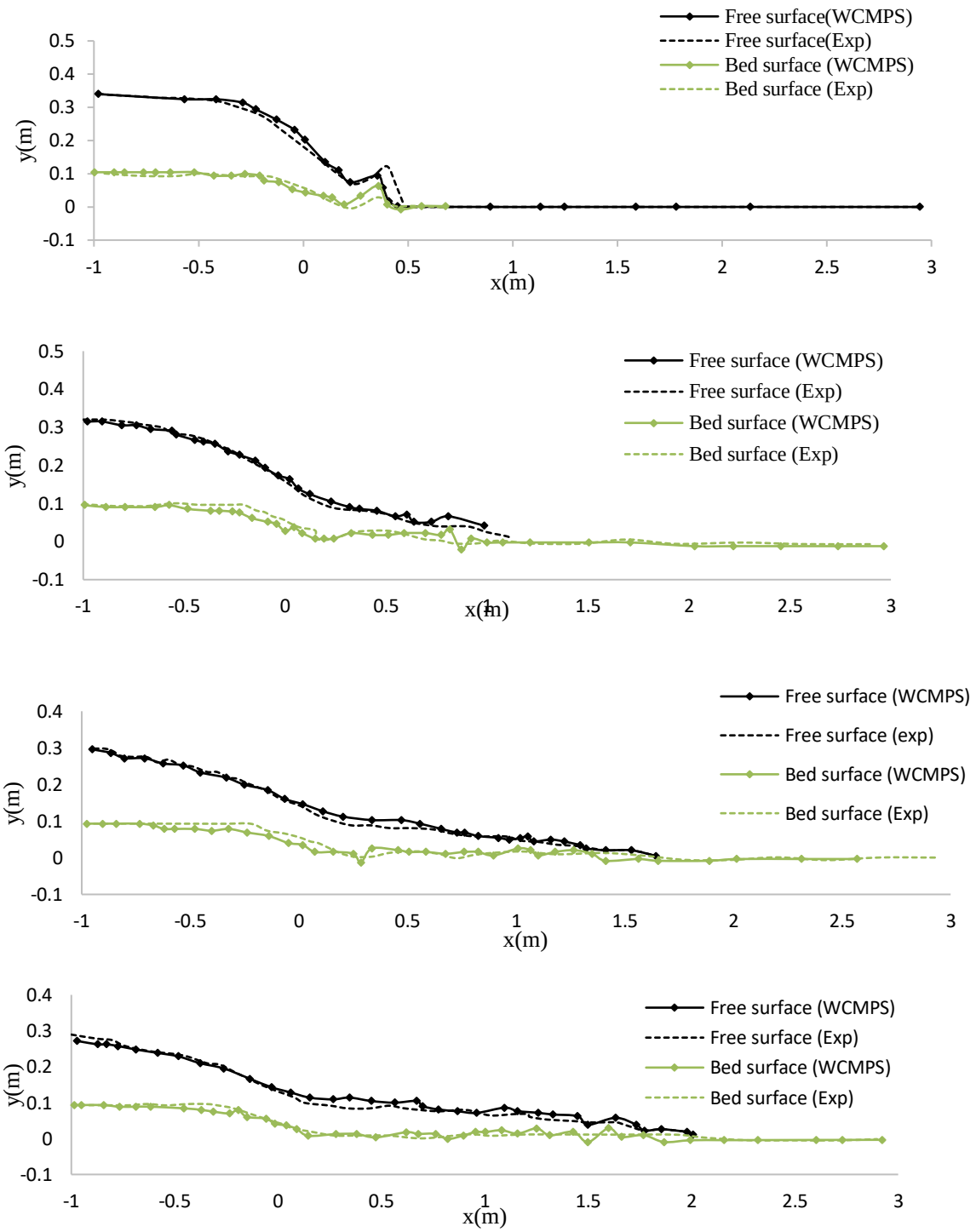


Fig. 8. Quantitative comparison of numerical and experimental water and sediment surface at t=0.25, 0.5, 0.75, and 1.0 seconds (case A)

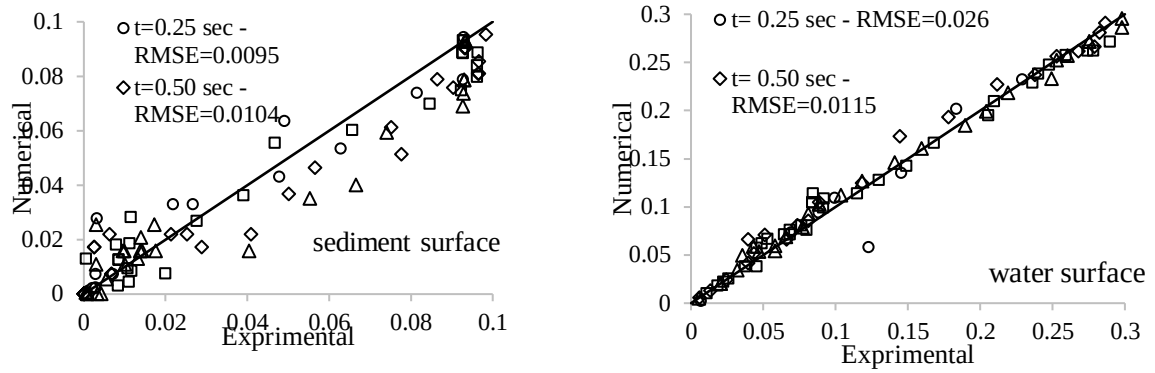


Fig. 9. The numerical method (WC-MPS) versus experimentally measured a) sediment surface and b) water surface

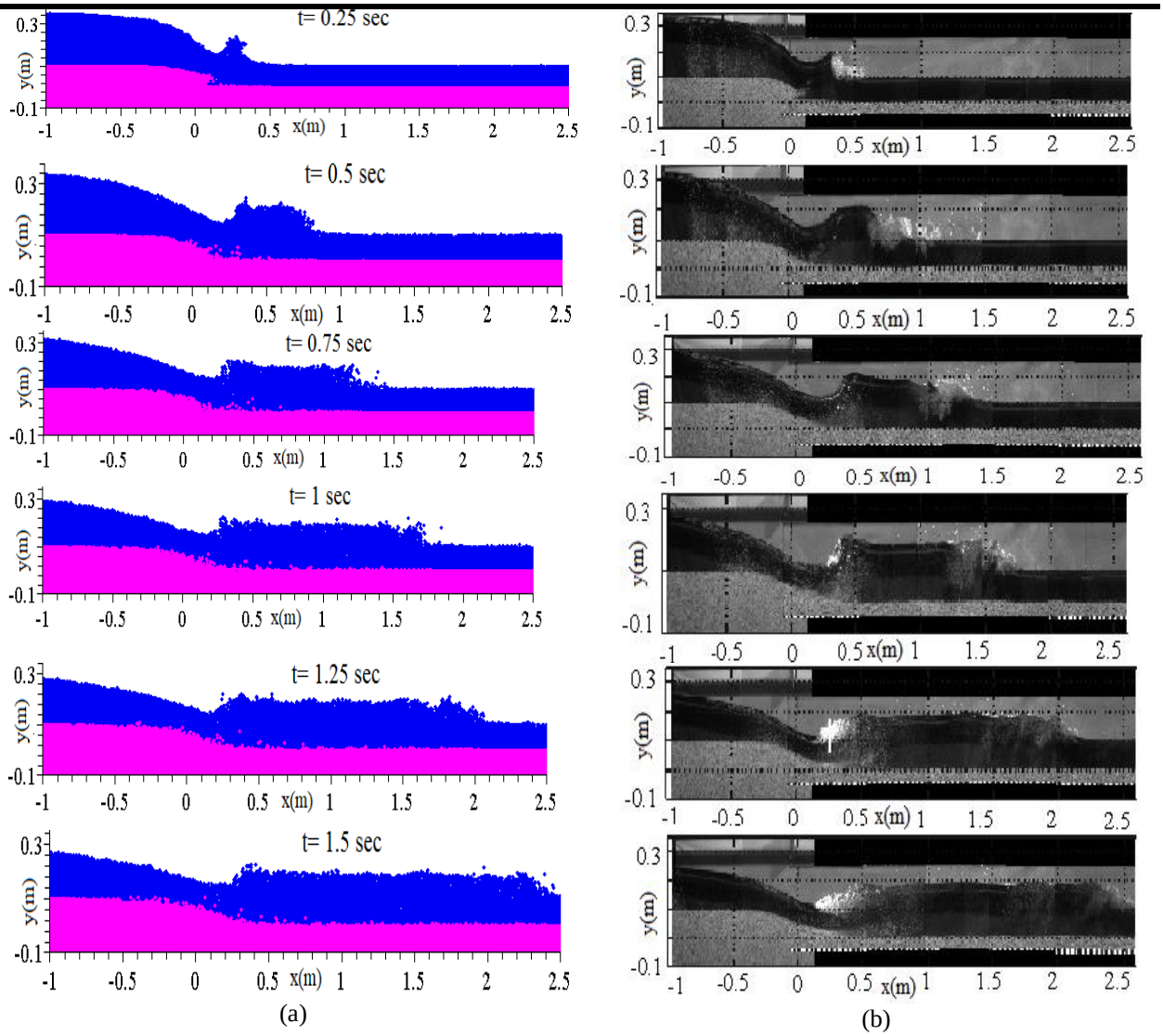


Fig. 10. (a) The numerical and (b) Experimental (Spinewine, 2005) snapshots of erodible-bed dam breaks (setup B)

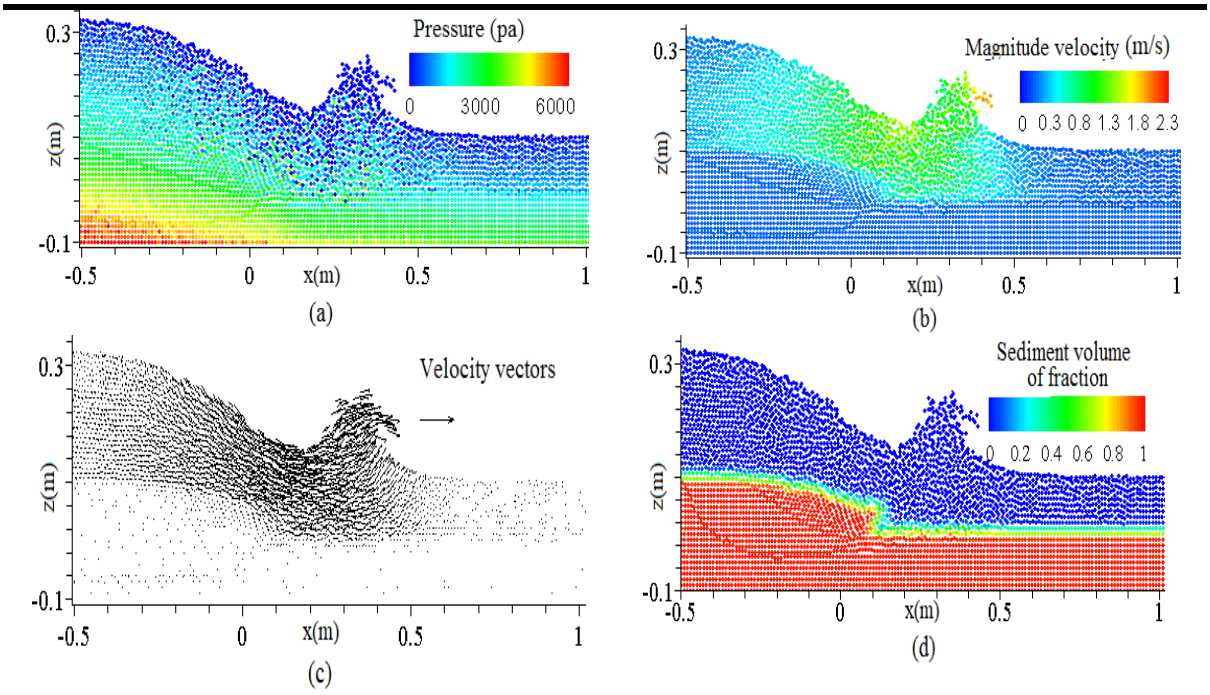


Fig. 11. (a) Pressure, (b) velocity magnitude, (c) velocity vector, and (d) volume fraction simulated at t=0.25 sec (setup B)

4. Conclusions

A mesh-free Lagrangian model, based on a weakly compressible MPS formulation, was developed and evaluated for the simulation of the two-phase rapid sediment transport. To model non-cohesive sediments, the sediment material was treated as a non-Newtonian visco-plastic fluid. The Herschel-Bulkley (H-B) rheological model (an exponentially-regularized version) in combination with Mohr-Coulomb yield criteria was used to predict the non-Newtonian behavior of sediment materials. The capability of the developed numerical method was evaluated for the two-phase sediment transport in a validation case, i.e. dam break on an erodible bed (for two geometries), and the results were compared with the available experimental measurements. Comparing the results with the experimental data showed the capabilities of the proposed model in the accurate prediction of sediment and water profiles for these sample problems. The results not only demonstrated the capability of the mesh-free particle method for rapid sediment transport modeling but also provided a better understanding of flow and sediment dynamics in the test cases of this study

5. Data Availability Statement

The datasets generated and/or analyzed during the current study are available upon reasonable request from the corresponding author.

6. References

1. Ataie-Ashtiani, B. and Farhadi, L. 2006. “A stable moving-particle semi-implicit method for free surface flows.” Fluid Dynamics Research, 38, 241-256.
2. Calantoni, J., Holland, K.T. and Drake, T.G. 2004. “Modelling sheet-flow sediment transport in wave-bottom boundary layers using discrete-element modeling. Philosophical Transactions-Royal Society of London.” Series A, Mathematical, Physical and Engineering Sciences, 362, 1987-2002.
3. Gingold, R.A. and Monaghan, J.J. 1977. “Smoothed particle hydrodynamics: Theory and application to non-spherical stars.” Monthly Notices on the Royal Astronomical Society, 181, 375-389
4. Gotoh, H. and Sakai, T. 2006. “Key issues in the particle method for computation of wave breaking.” Coastal Engineering Journal, 53(2-3), 171-179.
5. Hsu, T.J., Jenkins, J.T. and Liu, P.L.F. 2003. “On two-phase sediment transport: Dilute flow.” Journal of Geophysical Research (Oceans), 108, 14.
6. Jafari Nodoushan, E., Shakibaeinia, A. and Hosseini, Kh. 2018. “A multiphase meshfree particle method for continuum-based modeling of dry and submerged granular flows.” Powder Technology, 335, 258-274.
7. Jafari-Nodoushan, E. Hosseini, Kh. Shakibaeinia, A. Mousavi. S.F. 2016. “Meshless particle modelling of free surface flow over spillways.” Journal of Hydroinformatics, 18 (2): 354–370
8. Jafari Nodoushan, E. and Shakibaeinia, A. 2019. Multiphase mesh-free particle modeling of local sediment scouring with μ(I) rheology. Journal of Hydroanfomatics, 21(2), 279-294.

9. Jandaghian, M., Krimi, A., & Shakibaeinia, A. 2021. Enhanced weakly-compressible MPS method for immersed granular flows. Advances in Water Resources, 152, 103908.
10. Khayyer, A. and Gotoh, H. 2009. "Modified moving particle semi-implicit methods for the prediction of 2D wave impact pressure." Coastal Engineering Journal, 56, 419-440.
11. Khayyer, A. and Gotoh, H. 2010. "A higher order Laplacian model for enhancement and stabilization of pressure calculation by the MPS method." Applied Ocean Research, 32, 124-131.
12. Koshizuka, S., Tamako, H. and Oka, Y. 1995. "A particle method for incompressible viscous flow with fluid fragmentation." Computational Fluid Dynamics Journal, 4(1), 29-46.
13. Koshizuka, S. and Oka, Y. 1996. "Moving particle semi-implicit method for fragmentation of incompressible fluid." Nuclear Science and Engineering, 123(3), 421-434.
14. Manenti, S., Sibilla, S., Gallati, M., Agate, G. and Guandalini, R. 2011. "SPH simulation of sediment flushing induced by a rapid water flow." Journal of Hydraulic Engineering, 138(3), 272-284.
15. McTigue, D.F. 1981. "Mixture theory for suspended sediment transport." Journal of the Hydraulic Division, 107(6), 659-673.
16. Meyer-Peter, E. and Müller, R. (1948). "Formulas for bed-load transport." Proceedings of the 2nd Meeting of the International Association for Hydraulic Structures Research, pp. 39-64.
17. Mitsoulis, E. 2007. "Flows of viscoplastic materials" Models and computations. Rheology Reviews, the British Society of Rheology, pp. 135-178.
18. Papanastasiou, T.C. 1987. "Flows of materials with yield." Journal of Rheology, 31, 385-404.
19. Shakibaeinia, A. and Jin, Y.C. 2010. "A weakly compressible MPS method for simulation of open-boundary free-surface flow." International Journal for Numerical Methods in Fluids, 63(10), 1208-1232.
20. Shakibaeinia, A. and Jin, Y.C. 2011. "A mesh-free particle model for simulation of mobile-bed dam break." Advances in Water Resources, 34, 794-807.
21. Shakibaeinia, A. and Jin, Y.C. 2012a. "MPS mesh-free particle method for multiphase flows." Computer Methods in Applied Mechanics and Engineering, 229-232, 13-26.
22. Shakibaeinia, A. and Jin, Y.C. 2012b. "Lagrangian multiphase modeling of sand discharge into still water." Advances in Water Resources, 48, 55-67.
23. Spinewine, B. 2005. "Two-layer flow behaviour and the effects of granular dilatancy in dam break induced sheet-flow." PhD Thesis, Univerisité de Louvain.
24. Tajnesaie, M., Shakibaeinia, A., & Hosseini, K. 2018. "Meshfree particle numerical modelling of sub-aerial and submerged landslides." Computers & Fluids, 172, 109-121.
25. Van Rijn, L.C. 1984. "Sediment transport, part I: Bed load transport." Journal of Hydraulic Engineering, 110(10), 1431-1456.